Environmental Pollution 290 (2021) 118068

Contents lists available at ScienceDirect

Environmental Pollution

journal homepage: www.elsevier.com/locate/envpol

On the prediction of settling velocity for plastic particles of different shapes☆

Simona Francalanci *, Enio Paris, Luca Solari

Department of Civil and Environmental Engineering, University of Florence, Italy

ARTICLE INFO

Keywords:
Settling velocity
Transport processes
Plastic particle

ABSTRACT

Transport processes of plastic particles in freshwater and marine environments are one of the relevant advances of knowledge in predicting the fate of plastic in the environment. Here, we investigated the effect of different shapes on the settling velocity, finding a representative reference diameter which encompasses three-dimensional shapes like pellets or spherules, two-dimensional shapes like fragments or disks, and one-dimensional shapes like filaments or fibers. The new method is able to predict the settling velocity of plastic and natural particles given the representative size and the Corey shape factor coefficient, over the entire range of viscous to turbulent flow regime.

The calibration of the method with experimental data, and the validation with an independent dataset, support its application in a wide range of hydraulic conditions.

1. Introduction

The presence of plastic particles in freshwater and marine environment attracted an increasing attention in the scientific community during the last decade (Eriksen et al., 2014; Gasperi et al., 2014; Chubarenko et al., 2018; Lambert and Wagner, 2018): the fate of plastic particles in any aquatic environment is clearly related to transport processes occurring in the flow, but also to other processes such as the interaction with suspended sediment and dissolved salts, which can promote aggregation and settling (Li et al., 2019; Wang et al., 2020).

With respect to transport processes, settling velocity represents a fundamental property of particles being of great relevance as it allows evaluating the hydraulic threshold conditions between different modes of transport (i.e., incipient motion, bed-load, suspended-load) and thus the possible pathways and areas of accumulation of plastic particles in the various environmental compartments, i.e. the prediction of the fate of plastic particles in rivers.

Previous fundamental studies on the settling velocity W of natural particles (such as Dietrich, 1982, who collected previous studies on natural sediment, e.g. gravel or sand, smooth spheres and well rounded ellipsoids) demonstrated that W can be evaluated through empirical relationships as a function of properties of the fluid (density and viscosity), and density, size, shape, roundness, and surface texture of the particle.

The extension of previous formulations devised for natural particles to plastic particles is not trivial as the latter are characterized by a larger variety of shapes that include 2D (such as disks) and 1D (filaments, wires) geometries. Previous studies investigated the most suitable parameter to describe particle shape: i.e., Van Melkebeke et al. (2020) found that circularity and sphericity are appropriate shape descriptors for film particles; Dioguardi et al. (2017) used the sphericity for volcanic ash; Saxby et al. (2018) outlined the need of several shape factors and their dependences on particle size; Khatmullina and Isachenko (2017) used the ratio L/d for long cylinders. One of the main difficulties, encountered by previous studies, is related to the definition of a single reference diameter accounting both for the entire, often irregular, particle geometry and for the complex hydrodynamic processes that occur while the particle is falling through a fluid.

To overcome the ubiquitous irregularity of particle geometry, in many cases an equivalent sphere is assumed based on some physical property measured by the adopted technique (Switzer, 2013); examples include: equivalent sphere on the same measured particle volume, sphere based on the same surface area, sphere passing through the same sieve opening.

Regarding the hydrodynamic aspects, non-spherical particles can present different cross-sections depending on their orientation; while

☆ This paper has been recommended for acceptance by Baoshan Xing.

* Corresponding author.
E-mail address: simona.francalanci@unifi.it (S. Francalanci).

https://doi.org/10.1016/j.envpol.2021.118068
Received 1 May 2021; Received in revised form 26 August 2021; Accepted 28 August 2021
Available online 31 August 2021

falling through a fluid the most stable configuration is associated to the maximum projected area in the direction of particle motion (Middleton and Southard, 1978). However, particle orientation changes with hydraulic regime and the corresponding settling Reynolds number: in the Stokes regime the particle keeps its original orientation while sinking; on the contrary, in the transitional and turbulent flow regime, due to flow separation, wake formation and vortex shedding, particle might experience oscillations, rotation, and tumbles while falling almost parallel to its maximum projected area normal to the fall direction (Stringham et al., 1969; Komar and Reimers, 1978).

In the present work, we extend the previous analysis by Ferguson and Church (2004), originally formulated for evaluating fall velocity of natural particles, to plastic particles. We propose a comprehensive approach interpreting fall velocity of particles of any shapes (3D, 2D and 1D) in the various hydraulic regimes (covering low and high Reynolds number), while preserving its validity for natural particles. The theoretical approach is tested and validated using a large dataset that include both new evidence from laboratory experiments and previous experiments on natural (Le Roux, 2004) and plastic (Khatmullina and Isachenko, 2017; Van Melkebeke et al., 2020) particles.

2. Theoretical framework

According to the definition of settling velocity, the forces acting on a single particle falling in still fluid must be balanced. The gravity force acting during the sinking of particle is counterbalanced by a hydrodynamical force which will reach a constant value when the particle velocity becomes uniform, that is when the settling velocity is attained. Theoretical solution of the problem was provided by Stokes (1851) for spherical particle falling in an infinite calm fluid in the viscous flow regime.

For any particle shape of volume V [m^3] and density ρ_s [kg/m^3] the terms of force balance can be written:

$$g(\rho_s - \rho)V = \frac{\rho}{2} C_d w A \tag{1}$$

where: g, gravity acceleration [m/s^2]; ρ, fluid density [kg/m^3]; C_d, drag coefficient [-]; w, settling velocity [m/s]; A, projected area of the particle perpendicularly to the flow direction [m^2].

In eq. (1), the drag coefficient C_d is theoretically determined by the Stokes solution as a function of the Reynolds number $Re = wD/\nu$, where D is the diameter of a particle [m], and ν is the fluid kinematic viscosity [m^2/s]. Beyond the Stokes regime, for finite Reynolds numbers ($Re > 1$), inertial forces start to become significant and C_d is corrected by introducing additional factors related to the particle geometry (shape and roundness) and surface texture ε:

$$C_d = f(R_e,\ shape,\ roundness,\ \varepsilon) \tag{2}$$

Relationship (2) needs to be determined through experiments. For non-spherical particles, volume V and projected area A can be evaluated by introducing the nominal sphere-equivalent diameter, D_n, such that:

$$V = k_1 D_n;\ A = k_2 D_n \tag{3}$$

with k_1 and k_2 numerical coefficients varying with shape. Then eq. (1) can be written as:

$$g(\rho_s - \rho)k_1 D_n^3 = \frac{\rho}{2} C_d w^2 k_2 D_n^2 \tag{4}$$

and in terms of settling velocity:

$$w = \sqrt{2\frac{k_1}{k_2} g\left(\frac{\rho_s - \rho}{\rho}\right) \frac{D_n}{C_d}} \tag{5}$$

From eq. (5), it can be observed that settling velocity is a function of the shape, the characteristic size D_n, the drag coefficient C_d, and the submerged relative density $R = (\rho_s - \rho)/\rho$.

For spherical particles flowing in the viscous regime, Stokes solution provides the expression for the drag coefficient, $C_d = 24/Re$, showing that fall velocity varies as the square of particle size. Beyond the Stokes regime, i.e. for $Re > 1$, it has been observed that in the range $10^3 < Re < 10^5$ the drag coefficient C_d reaches a constant asymptotic value and the fall velocity, according to eq. (5), varies as the square root of particle size. Hence, it can be recognized the existence of two asymptotic regions of the settling velocity depending on the particle Reynolds number, i.e., the viscous region when $Re < 1$ and the turbulent region when $10^3 < Re < 10^5$. From the above considerations, it can be concluded that settling velocity is in general depending on the following variables:

$$w = f(D_n, R_e, R, shape, roundness, \varepsilon) \tag{6}$$

According to Dietrich (1982), the functional relationship (6) can be expressed in a non-dimensional form by introducing the following dimensionless parameters:

- fall velocity $W^* = \frac{w}{(gR\upsilon)^{1/3}}$
- reference particle size $D^* = D_n\left(\frac{gR}{\upsilon^2}\right)^{1/3}$
- Corey shape factor defined as $csf = \frac{c}{\sqrt{ab}}$

where a, b and c represent the longest, intermediate and shorted axis of each particle. csf takes values from nearly 0 (2D plate/disk) up to 1 (perfectly rounded 3D sphere), while $csf = 0.7$ for naturally worn sediment (Dietrich, 1982).

By observing that $R_e = W^* D^*$ and neglecting both the effects of ε and of roundness (Dietrich, 1982), eq. (6) can be expressed in dimensionless form as:

$$W^* = f(D^*,\ csf) \tag{7}$$

This functional relationship can be obtained by using experimental data and theoretical considerations, as described in the following sections.

2.1. Existing settling velocity equations

Most of the existing equations have been derived on the basis of eq. (5) by imposing the respect of the two asymptotic solutions previously described; however, some formulas do not take into account the effect of shape and roundness of particles (see for instance Soulsby, 1997; Cheng, 1997; Ahrens, 2000; Guo, 2002; Zhiyao et al., 2008), while others consider the effect of shape in the viscous regime (Komar and Reimers, 1978; Komar, 1980). More recently, Jiménez and Madsen (2003) proposed a formula where the shape and the roundness of the particles significantly affect the settling velocity, after resumed by Camenen (2007). Other approaches include implicit formulations which predict settling velocity fitting the drag coefficient across different flow regimes (Khan and Richardson, 1987; Song et al., 2017; Bagheri and Bonadonna, 2016; Waldschläger and Schüttrumpf, 2019).

Given the large amount of empirical, theoretical and experimental equations, the assessment of the performance of each formula is beyond the scope of the present work and already done in Literature (among the last works, see Van Melkebeke et al., 2020). However, we summarize here some of the approaches which will be used in the following for comparison purposes: Dietrich (1982), Ferguson and Church (2004), Camenen (2007), Khatmullina and Isachenko (2017), and Waldschläger and Schüttrumpf (2019).

The non-dimensional variables D^* and W^* were first introduced by Dietrich (1982) in his comprehensive work concerning the fall velocity of sediment particles. He outlined the different behaviour of irregularly shaped particles with respect to smooth spherical particles. Using experimental data, Dietrich proposed relationships to estimate the deviation from fall velocity of smooth spherical particles due to shape and roundness effects. The relationship for smooth spherical particle consists

of a fourth-order polynomial of log D^*:

$$\log(W^{*3}) = -3.76715 + 1.92944\log(D^{*3}) - 0.09815\log(D^{*3})^2 - 0.00575\log(D^{*3})^3 + -0.00056\log(D^{*3})^4 \quad (8)$$

Ferguson and Church (2004) derived a new equation using dimensional analysis and imposing the convergence to the Stokes law for small grains and to a constant drag coefficient for large grains. An explicit equation to provide the fall velocity over the entire range of viscous to turbulent conditions is proposed in the form:

$$w = \frac{gRD^2}{C_1\nu + \left(0.75C_2gRD^3\right)^{0.5}} \quad (9)$$

Eq (9) reduces to Stokes' law when the first term of the denominator is dominant with constant C_1 taking the values in the range 18–24, and the second term vanishes. Vice versa, in the turbulent flow regime the second term is prevailing and eq. (9) reduces to a constant drag coefficient where C_2 is in the range 0.4–1.2. Hence, the fall velocity varies as the square of particle size in the viscous regime while it varies as the square root in turbulent flow.

It must be outlined the simplicity of equation (9) while providing very similar results of Dietrich equation (1982). Equation (9) can be reformulated in terms of the W* and D* as follows:

$$W_* = \frac{D_*^2}{C_{1+}\sqrt{C_2 0.75 D_*^3}} \quad (10)$$

Camenen (2007) used a similar approach of the asymptotic fitting of the drag coefficient at low and high Reynolds numbers, deriving a simple and general formula for the settling velocity which takes into account different shape and roundness of particles. The equation reads:

$$w = \frac{\nu}{D}\left[\sqrt{\frac{1}{4}\left(\frac{A}{B}\right)^{2/m} + \left(\frac{4}{3}\frac{D^*}{B}\right)^{1/m}} - \frac{1}{2}\left(\frac{A}{B}\right)^{1/m}\right]^m \quad (11)$$

where the coefficient A, B and m vary according to the material:

$$A = a_1 + a_2\left[1 - sin\left(\frac{\pi}{2}csf\right)\right]^{a_3} \quad (12a)$$

$$B = b_1 + b_2\left[1 - sin\left(\frac{\pi}{2}csf\right)\right]^{b_3} \quad (12b)$$

$$m = m_1 sin^{m_2}\left(\frac{\pi}{2}csf\right) \quad (12c)$$

with $a_1 = 24$, $b_1 = 0.39 + 0.22$ (6-P); $m_1 = 1.2 + 0.12$P; $a_2 = 100$; $b_2 = 20$; $m_2 = 0.47$; $a_3 = 2.1 + 0.06$P; $b_3 = 1.75 + 0.35$P. P is the particle roundness which is estimated using the scale of Briggs et al. (1962), and varying from 0 (perfectly angular) to 6 (perfectly round), P = 2.0 for crushed grains and P = 3.5 for natural sand.

More recently, Khatmullina and Isachenko (2017) analysed the settling velocity of spheres, short cylinders and long cylinders made by Polycaprolactone (material density in the range 1131–1168 kg/m^3), showing the relevant deviation of settling velocity for elongated cylinders with respect to the predictions related to spheres and short cylinders. An equation for predicting the fall velocity of elongated cylinders, essentially having a 1D shape, is proposed in dimensional form as follows:

$$w = \frac{\pi}{2}\frac{1}{\upsilon}gR\frac{LD}{(55.238L + 12.691)}\frac{1}{1000} \quad (13)$$

where L (mm) and D (mm) are the length and diameter of the cylinder, respectively. It must be noted that eq. (13) is different from the original formulation (Khatmullina and Isachenko, 2017) which appears to be not consistent from a dimensional point of view; in particular the factor 1/1000 is here added to obtain a fall velocity in *mm/s* as originally specified.

Finally, we report here the approach by Waldschläger and Schüttrumpf (2019) who proposed different expression of the drag coefficient both for pellets and fragments, and for fibers, for settling and rise velocity of microplastics in freshwater environment. The equations for the settling case reads:

$$C_d(settling, pellets\ and\ fragments) = \left(\frac{3}{csf\cdot\sqrt[3]{Re}}\right) \quad (14)$$

$$C_d(settling, fibers) = \left(\frac{4.7}{\sqrt{Re}} + \sqrt{csf}\right) \quad (15)$$

3. Materials and methods

Methods include laboratory experiments where the falling velocity of plastic particles of different density and shape (3D and 2D) was evaluated, and the interpretation of these measurements using theoretical/analytical considerations.

3.1. Laboratory experiments

The experiments were carried-out in the laboratory of 'River, Lagoon Hydraulics and Biofluidodynamics' of the University of Florence.

The terminal fall velocity *w* of plastic samples (Table 1 and Fig. 1) was observed in a 1.7 m tall cylinder with a diameter of 0.08 m containing tap water at an average temperature of 18 °C. Measurements of particle travelling time were taken in the lower 1.2 m by using a camera and using horizontal marks placed on the tall cylinder every 20 cm (see Figure S1 in the supplementary material for a scheme of the experiments). Particles were previously immersed in water for about 10 min to ensure that they were properly wetted and without air bubbles. A total number of 168 particles was examined (see column N in Table 1); for each particle, the experimental tests were repeated 5 times, and the average value of fall velocity is ascribed to the particle.

Particle density was obtained by weighting simultaneously all the particles pertaining to each sample using a scale (precision 0.1 g) and by measuring their volume in a cylinder of water with a diameter of 1.5 cm after all air bubbles were released; this procedure was repeated 15 times for each sample.

The 10 samples analysed include 2D irregular fragments and 3D cylindrical pellets with densities ranging between 1040 and 1370 kg/m^3 and size ranging between 1.68 mm up to 5.44 mm (Table 1 and Fig. 1).

Table 1
Tested microplastics samples; *csf* is averaged over all the particles of each sample.

Sample #	Type [-]	Equivalent spherical diameter [mm]	Density [g/cm^3]	*csf* [-]	Shape [-]	N [-]
1	PVC	2.83–3.40	1084	0.85	3D regular pellets	15
2	PVC	3.37–4.94	1210	0.81	3D Regular Pellets	10
3	PVC	1.68–2.53	1250	0.25	3D regular pellets	13
4	PET	2.43–4.42	1100	0.10	2D Irregular fragments	30
5	PET	2.71–4.18	1150	0.03	2D Irregular fragments	4
6	PET	3.68–5.44	1150	0.07	2D Irregular fragments	6
7	PET	3.41–4.43	1370	0.79	3D Pellets	30
8	ABS	2.41–2.89	1040	0.65	3D regular pellets	30
9	PS	3.31–4.14	1030	0.80	3D regular pellets	15
10	PSC	2.59–3.29	1039	0.66	3D regular pellets	15

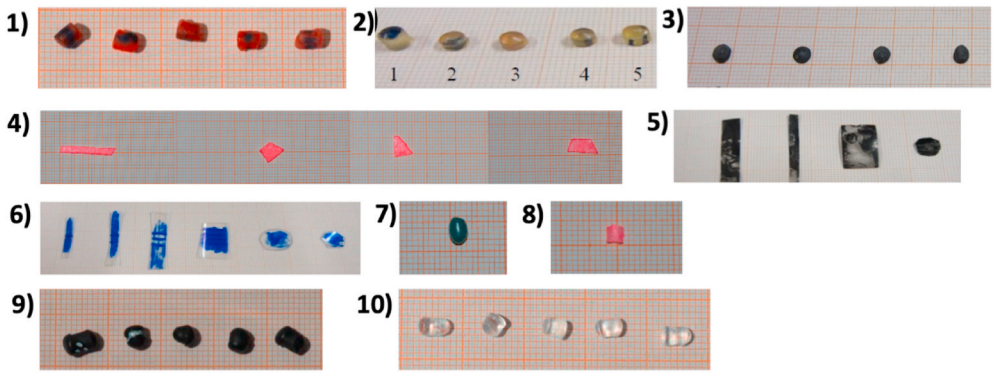

Fig. 1. Examples of microplastics tested in the hydraulics laboratory, using different type of polymers: PVC #1,# 2, #3; PET #4, #5, #6, #7; ABS #8; PS #9; PSC #10. The particle number N pertaining to each sample is reported in Table 1 (N total = 168).

Size of particles was determined by using a calliper (precision 1/20 mm). An extended dataset of the sample characteristics is reported in the Supplementary Material.

3.2. Development of the new method

A method able to describe the falling behavior of plastic particles based on a physically based equation, eq. (10), is here developed to provide predictions of general validity both in relation to the nature of the particles (natural sediment, plastic) and to their shape and flow regime.

To this aim, two main aspects need to be investigated: the definition of a reference size, and the definition of the asymptotic patterns in order to make eq. (10) of general validity.

As far as the reference size concerns, its definition is not obvious: many authors used as reference size the diameter of a sphere with the same volume and mass as the non-spherical grain (nominal diameter as in Le Roux, 2004), while in the case of 1D fibers or filaments Khatmullina and Isachenko (2017) did not propose any reference size since they used both the longest and the shortest axis length. The assumption made for the reference size plays a crucial role when comparing the different formulations. On the basis of a preliminary analysis of experimental data, we assumed that the reference size, in the following denoted as reference diameter, D_g, can be expressed as a function of axis ratio b/a and *csf*.

Regarding the asymptotic behaviour of fall velocity in the viscous regime, eq. (10) is extended following the approach proposed by Komar (1980) whereby the coefficient C_1 is corrected to take into account the shape effect as follows:

$$C_1 = 18 \cdot E^{-0.38} \tag{16}$$

with E the following shape factor:

$$E = a\left(\frac{a^2 + b^2 + c^2}{3}\right)^{-1/2} \tag{17}$$

For turbulent flow where secondary motion (i.e. tumbling, tipping, sliding) is greatly affecting the settling velocity, a new correction is here introduced in the second term of the denominator of eq. (10), by reformulating this equation as follows:

$$W_* = \frac{D_*^2}{C_1 + \left(0.75 C_2 D_*^3\right)^n} \tag{18}$$

where C_2 and n are assumed to be both a function of particle shape to be determined using the experimental data. Of course, for spherical particle the original values $C_2 = 0.4$–1 and n = 0.5 must be obtained.

3.3. Independent dataset

Three additional independent datasets were used in the present analysis for comparison with the proposed new method. We used the collection of data reported in Le Roux (2004), Khatmullina and Isachenko (2017), and Van Melkebeke et al. (2020).

In particular, Le Roux (2004) reported a set of 233 data, collected from a number of authors and concerning settling data of particles of various density and shape in both the laminar and turbulent regimes. These data are sorted according to their shape in 6 Tables; in particular: Table 1 with 49 data of ellipsoids (from Komar and Reimers, 1978); Table 2 with 39 data of spheres and spheroids (from Gibbs et al., 1971; Williams, 1966; Stringham et al., 1969); Table 3 with 35 data of prolate spheroids (from Stringham et al., 1969; Komar 1980; Williams, 1966); Table 4 with 36 data of oblate spheroids (from Stringham et al., 1969); Table 5 with 23 data of discs (from Stringham et al., 1969; Williams, 1966) and Table 6 with 51 data of cylinders and rods (from Komar 1980; Stringham et al., 1969).

Khatmullina and Isachenko (2017) used in their experiments spherical granules and cylinder-shaped granules made by Polycaprolactone plastic (material density 1131 kg/m^3), and pieces of fishing lines (with diameters in the range 0.15–0.71 mm, and densities 1130–1168 kg/m^3) with different lengths in the range 0.5–5 mm. The dataset used for comparison consisted of 123 data, chosen in the existence range of the formula given by equation (12), with combination of diameters ranging 0.13–0.87 mm and lengths from 1 to 6 mm.

Van Melkebeke et al. (2020) analysed the sinking behavior of typical microplastics originating from real plastic samples, generated from municipal plastic waste; the dataset is composed of 140 different microplastic particle from seven product type chosen on their frequency of occurrence and different shape class: granular or fragment shape (PET, HDPE, PP, PS with material density 952–1370 kg/m^3), film shape (PE with density 950–1013 kg/m^3), fiber (PVC with density 1432 kg/m^3). The data used as independent sets are reported in the Supplementary Material, for reader convenience.

4. Results

4.1. The reference diameter

Fig. 2 shows the experimental data (our data, Le Roux data, Khatmullina and Isachenko data) plotted in terms of b/a and Dn/a, where Dn is the nominal sphere-equivalent diameter: data are grouped according to the *csf* parameter spanning from almost 0 to 1, showing evidence of the dependence of Dn/a ratio with the *csf* parameter. It is worth to note the general trend of the Dn/a ratio to increase as b/a increases, with an increasing rate which progressively reduces as *csf* decreases. Moreover, the pattern of the experimental Dn/a ratio values correctly tend to 1 as

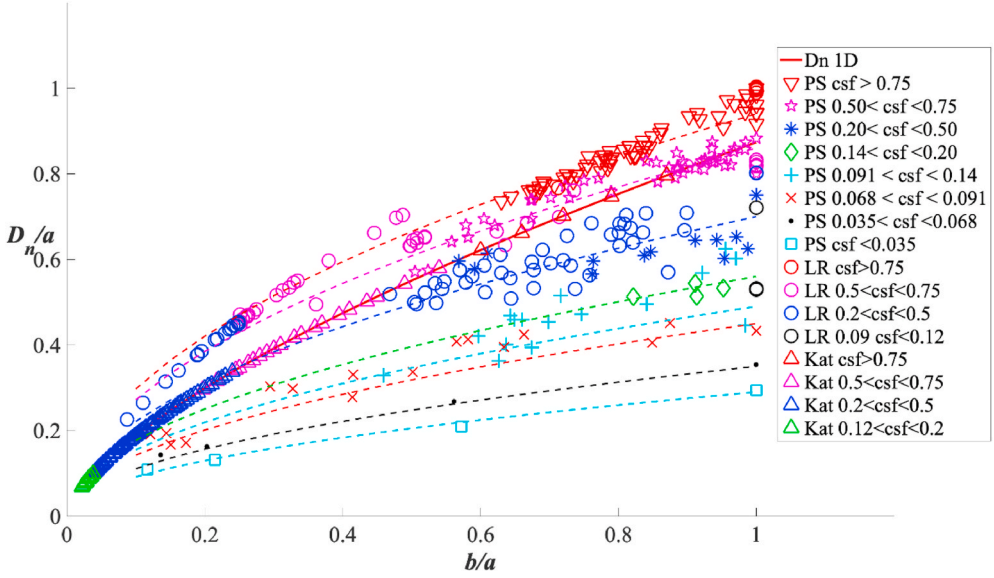

Fig. 2. Dimensionless nominal diameter D_n versus the axis ratio b/a grouped for different Corey shape factor (PS = Present Study, LR = Le Roux (2004), Kat = Khatmullina and Isachenko (2017)). The solid line "*Dn 1D*" is the geometrical relationship for the nominal diameter of 1D filament shape; the dashed lines represent the best fitting interpolation of the modified diameter D_g for the different groups of data according to *csf* parameter.

b/a and *csf* tend to 1. The relation for the reference diameter of 1D particle shape ("*Dn 1D*" line in Fig. 2), calculated on a geometrical base considering 1D particles shaped like long cylinder, is reported for comparison, and it clearly overlaps with the 1D dataset by Khatmullina and Isachenko (2017).

The experimental data grouped with increasing values of *csf* are used to fit a unique predictive equation (dashed lines in Fig. 2), derived from the best fitting of D_n/a and b/a data, using *csf* as parameter:

$$\frac{D_g}{a} = (csf)^{0.34}\left(\frac{b}{a}\right)^{0.5} \tag{19}$$

D_g is a "modified" diameter in the sense that it encompasses shape type, ant it is expressed in dimensionless form as a joint function of *csf* and the square root of *b/a*. The exponent 0.34 in eq. (19) was estimated by best fitting of the eight values of the interpolating curves of D_g/a in b/a = 1, for each *csf* group: the power relationship f $(csf)_{|b/a\,=\,1} = (csf)^{0.34}$ attains to a correlation coefficient $R^2 = 0.99$. D_g is to be used as reference diameter in the development of the new equations.

4.2. The asymptotic pattern in turbulent regime

Our experimental data pertaining to sample #1 to #10 in Table 1, have been classified according to the Corey shape factor *csf* and plotted in the diagram W*-D*modified (Fig. 3): the data corresponding to *csf*>0.5 arrange close to the curve by Ferguson and Church (2004), while the data with lower *csf* fall well below the curve. Alternative

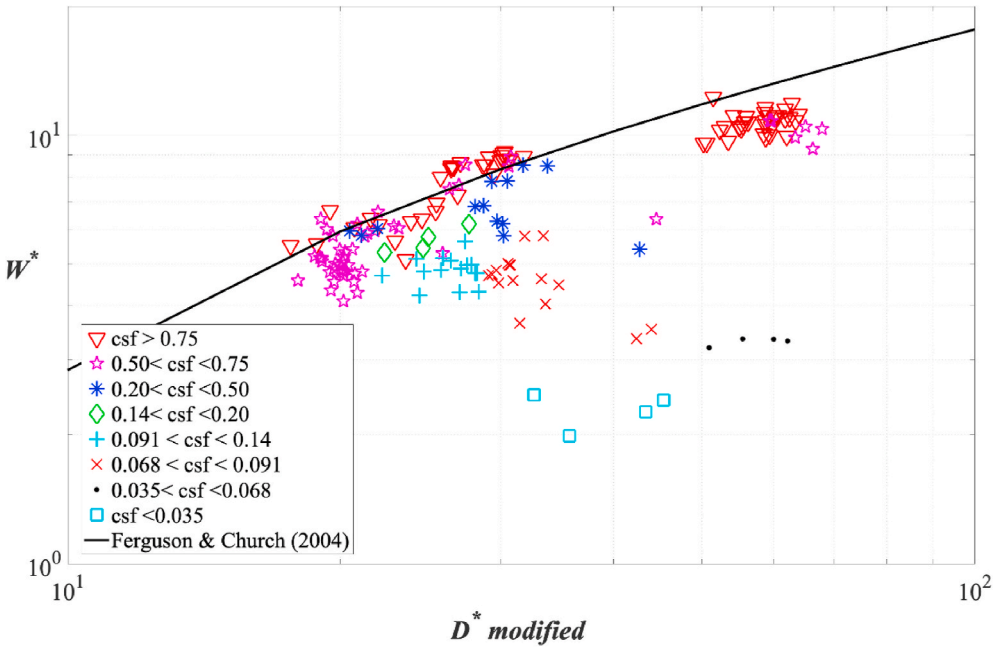

Fig. 3. Dimensionless fall velocity as a function of the modified dimensionless diameter: the present experimental data are illustrated; the solid line is equation (9) by Ferguson and Church (2004) valid for spherical particles (assuming $C_1 = 18$, $C_2 = 0.4$).

classification of the experimental data was investigated using other parameters, such as sphericity (Wadell, 1935) or E factor (Janke, 1966), but the Corey shape factor showed the best classifications.

Eight classes were defined covering the entire range of *csf*; in this way, the parameters C_2 and n in the turbulent regime for the general formulation of equation (18) (Fig. 4) were calibrated; the equation by Ferguson and Church (2004) for spherical particles is added to the plot, using $C_1 = 18$ and $C_2 = 0.4$ in equation (9).

For each group of data we calculated the correlation coefficient (R^2), the Nash Sutcliffe Efficiency coefficient (NSE) and the Index of Agreement (Ia): they were found close to one for the two groups with *csf*>0.5 ($R^2 = 0.77$, NSE = 0.78 and Ia = 0.94 for 0.50 < *csf*<0.75; $R^2 = 0.76$, NSE = 0.75 and Ia = 0.95 for *csf*>0.75), the other groups of data were composed by too few elements and these statistical parameters were not significant. The best fitting of the parameters of eq. (18) for each group of data is reported in the Supplementary Material (Figure S2-S7).

Through the analysis of the best fitting parameters for the experimental data, the following relationships for f_1 and f_2 have been derived (see the least square fitting in Fig. 5a and b):

$$C_2 = 0.3708 \cdot csf^{-0.1602} \tag{20}$$

$$n = 0.4942 \cdot csf^{-0.059} \tag{21}$$

Eqs. (20) and (21) correctly tend to the values $C_2 = 0.4$ and n = 0.5 of the original equation (10) when *csf* tends to 1.

The set of equations (18)–(21) constitutes a new general method for predicting settling velocity for particles of different size, shape, density for a wide range of hydraulic conditions. In Fig. 6 the comparison between experimental values of fall velocity versus predicted values obtained using equations (18)–(21): the values falling outside the range ± 30% of the line of perfect agreement are less than 10% over a total number of 168 measurements.

4.3. Independent test

Independent test of equations (17)–(20) was performed using the other three datasets introduced in section 3.3, which include a total number of measurements equal to 496. The results are shown in Fig. 7 where observed versus predicted values have been plotted using datasets of Le Roux (2004), Khatmullina and Isachenko (2017) and Van Melkebeke et al. (2020). It can be seen a general good performance of the proposed method able to predict fall velocity values within the range of ± 30% of perfect agreement for the 55% of data by Le Roux (2004) and Khatmullina and Isachenko (2017): in particular, data by Le Roux fall between the range of optimal agreement at the right and left ends, while on the middle of the graph the observed values are overestimated for *csf*>0.5 and underestimated for *csf*<0.14; data by Khatmullina and Isachenko are in general slightly overpredicted by the new formulation. Finally, the dataset by Melkebeke is in general overpredicted by the new formulation within a factor of two, which can be accepted as a reasonable estimate, given the high variability of particle shape (fragment, fiber, and film) and density uncertainty of real plastic waste.

Finally, it is useful comparing the prediction capability of different formulas in the literature, using the same set of data (Present study, LR, Kat, MEL); in Fig. 8 four selected formulas were applied to the dataset: Dietrich (1982), Camenen (2007), Waldschlager and Schuttrumpf (2019), and the new method of the present study. The data are reported in Fig. 8 grouped according to the value of *csf*.

The formula by Dietrich (1982) is a good predictor for regular shape particle, but it loses accuracy as the *csf* diminishes, overpredicting data with low values of *csf*, especially *csf*<0.15. The formula by Camenen (2007) is a good predictor at the edges for low and high fall velocity, while it does not perform well in the intermediate range of observed velocities. The formula by Waldschlager and Schuttrumpf (2019) seems to provide acceptable results only for a restricted amount of data, while values of *csf*<0.1 are on average underpredicted. Finally, the proposed approach enhances the prediction capability for regular particles at low and high fall velocity, while including good prediction for a wide range of *csf* values; it is right to note that particles with very low *csf* (<0.068) are slightly overpredicted by a factor of two.

5. Discussion

The main limitations of the present approach are related to the following aspects:

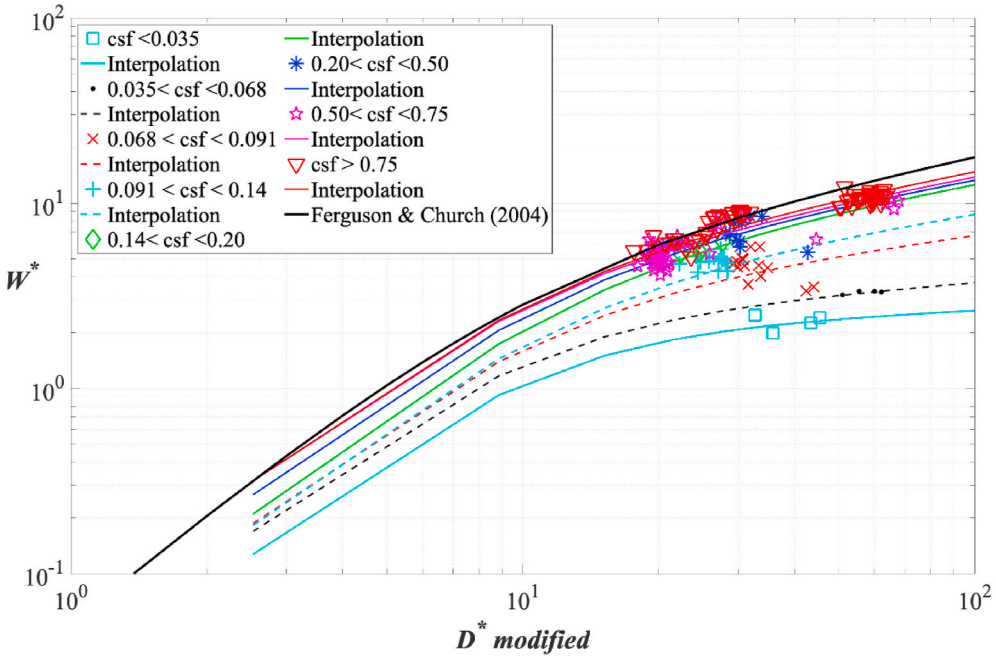

Fig. 4. New equation for dimensionless fall velocity as a function of modified dimensionless diameter: each group of data from the present study is interpreted with a best fitting interpolation line; the solid line is equation (9) by Ferguson and Church (2004) valid for spherical particles (assuming $C_1 = 18$, $C_2 = 0.4$).

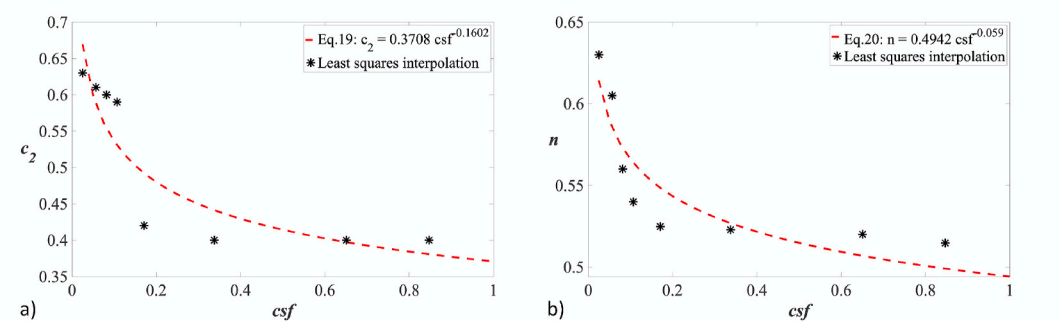

Fig. 5. Fitting of the parameters C_2 and n: the dots represent the parameter from the least square interpolation of the curves in Fig. 4, the dashed lines represent equations (19) and (20), respectively for C_2 and n.

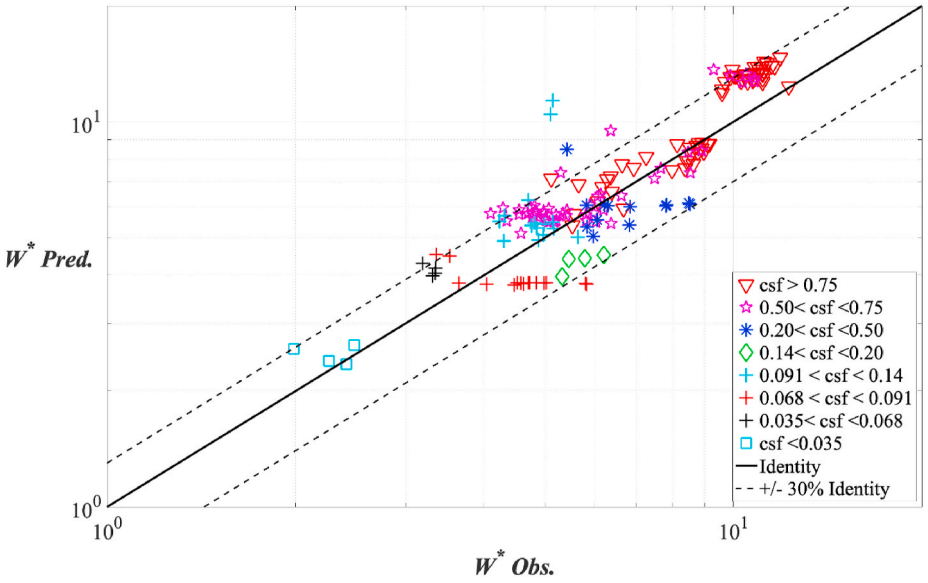

Fig. 6. Predicted versus observed dimensionless velocity, using the new developed method applied to the dataset collected in the Present Study; the solid line is the Identity, the dashed lines are Identity ± 30%.

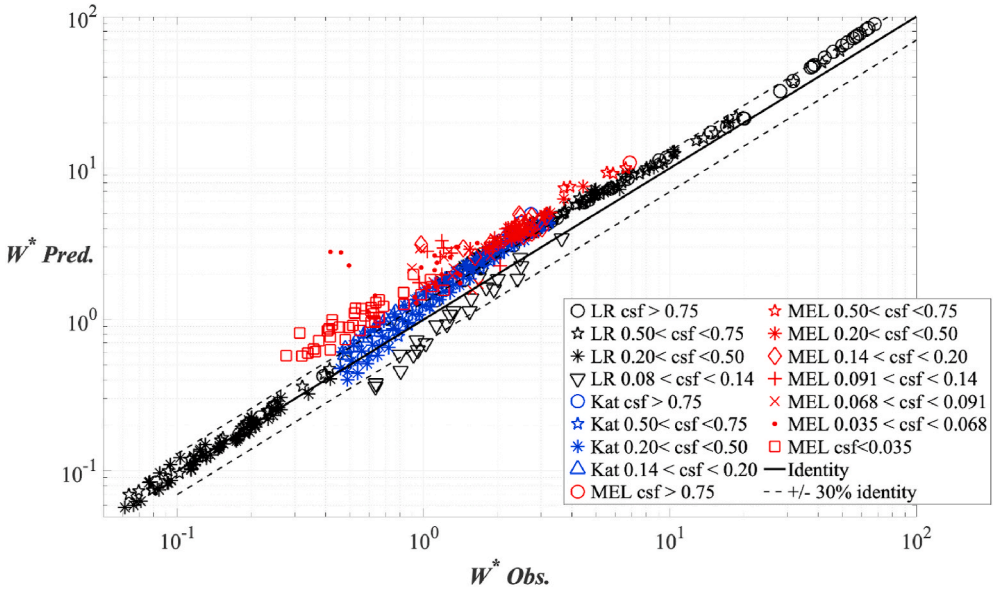

Fig. 7. Independent test of predicted versus observed dimensionless velocity using the new developed method, applied to the dataset by Le Roux (2004), Khatmullina and Isachenko (2017), and Van Melkebeke et al. (2020) respectively "LR", "Kat", and "MEL" in the legend.

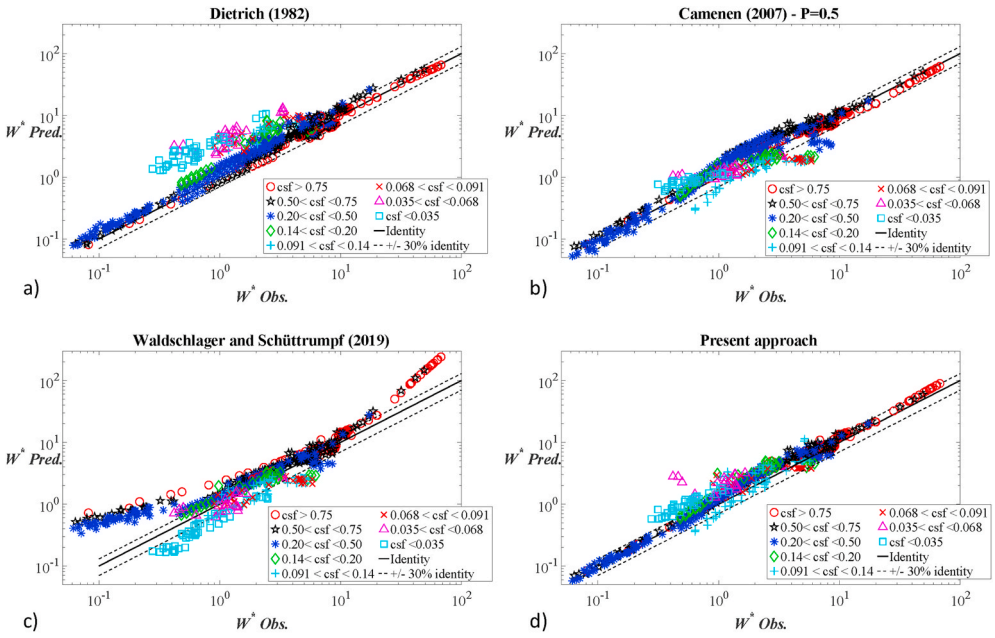

Fig. 8. Predicted versus observed dimensionless velocity: comparison for the three formulas by a) Dietrich (1982), b) Camenen (2007), c) Waldschlager and Schuttrumpf (2019), and d) Present approach.

- our analysis considers the settling of particles in quiescent fluids; in case of turbulent flows, particle fall velocity might be significantly altered (e.g., Good et al., 2014; Fornari et al., 2016) due to additional various processes such as the preferential sweeping mechanism (Maxey, 1987; Tom and Bragg, 2019; Li et al., 2021).
- Our method models the process of settling of solitary particles and therefore it does not include the flow disturbances produced by other (if any) neighboring particles (e.g., Uhlmann and Doychev, 2014). For that reason, its validity is limited to regimes when the particle concentrations are small enough to neglect such neighboring effects.
- Our method does not consider biofouling, which alters the polarity of plastic significantly and thereby influences the aggregation of plastic particles with other natural particles, subsequently giving a contribution to the settling motion of initially floating microplastics based on density modification (Van Melkebeke et al., 2020).
- Deformability of plastic particles during falling is not taken in account, but it was shown to be relevant for weathered film particles, affecting the transport behaviour in the aquatic environment (Waldschläger et al., 2020).

Considering the above limitations, the proposed approach outlines as a simple and explicit predictor for particle settling velocity, to be included in more complex transport modelling. It can be applied to a wide range of plastic shape, sizes and composition, with the exclusion of weathered and deformable particles.

Future improvements of the proposed formulation will consider an update in the definition of the particle reference size which should include not only the “geometry” of particles, but also the dynamic behaviour during particle settlement, which differs substantially in viscous or turbulent regime due to the secondary motion (tumbling, oscillating); also, the effect of surface coatings and deformability will be considered as further improvements.

6. Conclusion

This paper proposes a new method for predicting the settling velocity of plastic particles characterized by different shapes (3D, 2D and 1D). The new method has been developed by extending a previous formulation by Ferguson and Church, eq. (9), which applies to the entire range of viscous to turbulent flow regime. In fact, the formulation has a structure physically interpretable which can be adapted to take into account the effects of shape in both flow regimes. Using the experimental observations conducted in the present study, eq. (9) has been modified to adjust the viscous and the turbulent asymptotes as a function of particle shape. The Corey Shape Factor coefficient (*csf*) was confirmed to be one of the best suitable parameters for describing particle shape, assuming values below 0.5 for particles shaped like 2D disks or 1D fragments, and values toward 1 for particles shaped like 3D pellets, granules and spheres. Moreover, a unifying approach is proposed to estimate the reference size by introducing a “modified” equivalent diameter, eq. (19), based on the geometric characteristic of particles (essentially the longest, intermediate and shortest axis of the particle). Independent test, and comparison with other formulas from literature confirm the validity of the proposed method, eqs. (18)–(21), to predict fall velocities in a wide range of flow regime and particle characteristics.

However, a further improvement of the present approach for the definition of the reference size cannot be based only on particle geometrical properties, but it should include somehow the hydrodynamic interaction with flow.

Declaration of competing interest

The authors declare that they have no known competing financial interests or personal relationships that could have appeared to influence the work reported in this paper.

Acknowledgments

The authors received partial funding within the project "Plastics in the Arno River in Florence: concentration, transport and impacts" (Fondazione CR Firenze, 2020).

Appendix A. Supplementary data

Supplementary data to this article can be found online at https://doi.org/10.1016/j.envpol.2021.118068.

Author statement

The authors declare that the research article has not been published previously (except in the form of an abstract), that it is not under consideration for publication elsewhere, that its publication is approved by all authors and tacitly or explicitly by the responsible authorities where the work was carried out, and that, if accepted, it will not be published elsewhere in the same form, in English or in any other language, including electronically without the written consent of the copyright-holder.

References

Ahrens, J., 2000. A fall-velocity equation. J. Waterw. Port, Coast. Ocean Eng. 126 (2), 99–102.

Bagheri, G., Bonadonna, C., 2016. On the drag of freely falling non-spherical particle. Powder Technol. 301, 526–544. https://doi.org/10.1016/j.powtec.2016.06.015.

Briggs, L., McCulloch, D., Moser, F., 1962. The hydraulic shape of sand particles. J. Sediment. Petrol. 32 (4), 645–656.

Camenen, B., 2007. Simple and general formula for the settling velocity of particles. J. Hydraul. Eng. 133, 229–233. https://doi.org/10.1061/(ASCE)0733-9429(2007)133:2(229).

Cheng, N.-S., 1997. Simplified settling velocity formula for sediment particle. J. Hydraul. Eng. 123 (2), 149–152.

Chubarenko, I., Esiukova, E., Andrei Bagaev, A., Isachenko, I., Demchenko, N., Zobkov, M., Efimova, I., Bagaeva, M., Khatmullina, L., 2018. In: Zeng, Eddy Y. (Ed.), Behavior of Microplastics in Coastal Zones" in "Microplastic Contamination in Aquatic Environments. Elsevier.

Dietrich, W.E., 1982. Settling velocity of natural particles. Water Resour. Res. 18 (6), 1615–1626. https://doi.org/10.1029/WR018i006p01615.

Dioguardi, F., Mele, D., Dellino, P., Dürig, T., 2017. The terminal velocity of volcanic particles with shape obtained from 3D X-ray microtomography. J. Volcanol. Geoth. Res. 329 (2017), 41–53.

Eriksen, M., Lebreton, L.C.M., Thiel, M., Moore, C.J., Borerro, J.C., Galgani, F., Ryna, P. G., Reisser, J., 2014. "Plastic pollution in the world's oceans: more than 5 trillion plastic pieces weighing over 250,000 tons afloat at sea". PloS One 9 (12), 1–15. https://doi.org/10.1371/journal.pone.0111913.

Ferguson, R.I., Church, M., 2004. A simple universal equation for grain settling velocity. J. Sediment. Res. 74, 933–937. https://doi.org/10.1306/051204740933.

Fornari, W., Picano, F., Sardina, G., Brandt, L., 2016. Reduced particle settling speed in turbulence. J. Fluid Mech. 808, 153–167. https://doi.org/10.1017/jfm.2016.648.

Gasperi, J., Dris, R., Bonin, T., Rocher, V., Tassin, B., 2014. Assessment of floating plastic debris in surface water along the Seine. Environ. Pollut. 195, 163–166.

Gibbs, R.J., Matthews, M.D., Link, D.A., 1971. The relationship between sphere size and settling velocity. J. Sediment. Res. 41 (1), 7–18. https://doi.org/10.1306/74D721D0-2B21-11D7-8648000102C1865D.

Good, G., Ireland, P., Bewley, G., Bodenschatz, E., Collins, L., Warhaft, Z., 2014. Settling regimes of inertial particles in isotropic turbulence. J. Fluid Mech. 759, R3. https://doi.org/10.1017/jfm.2014.602.

Guo, J., 2002. Logarithmic matching and its applications in computational hydraulics and sediment transport. J. Hydraul. Res. 40 (5), 555–565.

Janke, N.C., 1966. Effect of shape upon the settling vellocity of regular convex geometric particles. J. Sediment. Res. 36 (2), 370–376. https://doi.org/10.1306/74D714C4-2B21-11D7-8648000102C1865D, 1966.

Jiménez, J.A., Madsen, O.S., 2003. A simple formula to estimate settling velocity of natural sediments. J. Waterw. Port, Coast. Ocean Eng. 129 (2).

Khan, A.R., Richardson, J.F., 1987. The resistance to motion of a solid sphere in a fluid. Chem. Eng. Commun. 62, 135–150. https://doi.org/10.1080/00986448708912056.

Khatmullina, L., Isachenko, I., 2017. Settling velocity of microplastic particles of regular shapes. Mar. Pollut. Bull. 114, 871–880. https://doi.org/10.1016/j.marpolbul.2016.11.024.

Komar, P., 1980. Settling velocities of circular cylinders at low Reynolds numbers. J. Geol. 88 (3), 327–336. http://www.jstor.org/stable/30062453.

Komar, P.D., Reimers, C.E., 1978. Grain shape effects on settling rates. J. Geol. 86, 193–209. https://doi.org/10.1086/649674.

Lambert, S., Wagner, M., 2018. Microplastics are contaminants of emerging concern in freshwater environments: an overview. In: Wagner, M., Lambert, S. (Eds.), Freshwater Microplastics. The Handbook of Environmental Chemistry, vol. 58. Springer, Cham.

Le Roux, J.P., 2004. A hydrodynamic classification of grain shapes. J. Sediment. Res. 74, 135–143.

Li, Y., Wang, X., Fu, W., Xia, X., Liu, C., Min, J., Zhang, W., Crittenden, J.C., 2019. Interactions between nano/micro plastics and suspended sediment in water: implications on aggregation and settling. Water Res. 161, 486–495. https://doi.org/10.1016/j.watres.2019.06.018, 2019.

Li, C., Lim, K., Berk, T., Abraham, A., Heisel, M., Guala, M., Coletti, F., Hong, J., 2021. Settling and clustering of snow particles in atmospheric turbulence. J. Fluid Mech. 912, A49. https://doi.org/10.1017/jfm.2020.1153.

Maxey, M., 1987. The gravitational settling of aerosol particles in homogeneous turbulence and random flow fields. J. Fluid Mech. 174, 441–465. https://doi.org/10.1017/S0022112087000193.

Middleton, G.V., Southard, J.B., 1978. Mechanics of Sediment Movement. Lecture Notes for Short Course, vol. 3. Eastern Section of the Soc. of Econ. Paleontol. and Mineralog., Binghampton, NY, p. 248.

Saxby, J., Beckett, F., Cashman, K., Rust, A., Tennant, E., 2018. The impact of particle shape on fall velocity: implications for volcanic ash dispersion modelling. J. Volcanol. Geoth. Res. 362 (2018), 32–48.

Song, X., Xu, Z., Li, G., Pang, Z., Zhu, Z., 2017. A new model for predicting drag coefficient and settling velocity of spherical and non-spherical particle in Newtonian fluid. Powder Technol. 321, 242–250. https://doi.org/10.1016/j.powtec.2017.08.017.

Soulsby, R.L., 1997. Dynamics of marine sands: a manual for practical applications. Oceanogr. Lit. Rev. 44 (9), 947, 1997.

Stokes, G.G., 1851. On the Effect of the Internal Friction of Fluids on the Motion of Pendulums, vol. IX. Transaction of the Cambridge Philosophical Society, p. 8.

Stringham, G.E., Simons, D.B., Guy, H.P., 1969. The Behavior of Large Particles Falling in Quiescent Liquids. Sediment Transport in Alluvial Channels. U.S. Geological Survey Professional Paper 562-C, p. 36.

Switzer, A.D., 2013. Measuring and analyzing particle size in a geomorphic context. In: Shroder (Ed. in Chif), J., Switzer, A.D., Kennedy, D.M. (Eds.), Treatise on Geomorphology, vol. 14. Academic Press, San Diego, CA, pp. 224–242. Methods in Geomorphology.

Tom, J., Bragg, A., 2019. Multiscale preferential sweeping of particles settling in turbulence. J. Fluid Mech. 871, 244–270. https://doi.org/10.1017/jfm.2019.337.

Uhlmann, M., Doychev, T., 2014. Sedimentation of a dilute suspension of rigid spheres at intermediate Galileo numbers: the effect of clustering upon the particle motion. J. Fluid Mech. 752, 310–348. https://doi.org/10.1017/jfm.2014.330.

Van Melkebeke, M., Janssen, C., De Meester, S., 2020. Characteristics and sinking behavior of typical microplastics including the potential effect of biofouling: implications for remediation. Environ. Sci. Technol. 54, 8668–8680, 2020.

Wadell, H., 1935. Volume, shape, and roundness of Quartz particles. J. Geol. 43 (3), 1935. https://doi.org/10.1086/624298.

Waldschlager, K., Schüttrumpf, H., 2019. Effects of particle properties on the settling and rise velocities of microplastics in freshwater under laboratory conditions. Environ. Sci. Technol. 53 https://doi.org/10.1021/acs.est.8b06794, 1958–1966.

Waldschläger, K., Born, M., Cowger, W., Gray, A., Schüttrumpf, H., 2020. Settling and rising velocities of environmentally weathered micro- and macroplastic particles. Environ. Res. 191 (2020), 110192. https://doi.org/10.1016/j.envres.2020.110192.

Wang, X., Li, Y., Zhao, J., Xia, X., Shi, X., Duana, J., Zhang, W., 2020. UV-induced aggregation of polystyrene nanoplastics: effects of radicals, surface functional groups and electrolyte. Environ. Sci.: Nano 7, 3914–3926. https://doi.org/10.1039/D0EN00518E, 2020.

Williams, G.P., 1966. Particle roundness and surface texture effects on fall velocity. J. Sediment. Petrol. 36, 255–259.

Zhiyao, S., Tingting, W., Fumin, X., Ruijie, L., 2008. A simple formula for predicting settling velocity of sediment particles. Water Sci. Eng. 1, 37–43. https://doi.org/10.1016/S1674-2370(15)30017-X.